Applied Physics Letters ARTICLE scitation.org/journal/apl

A large enhancement of ionic conductivity in $SrCoO_{2.5}$ controlled by isostructural phase transition and negative linear compressibility

Cite as: Appl. Phys. Lett. **119**, 043902 (2021); doi: 10.1063/5.0053978
Submitted: 13 April 2021 · Accepted: 26 June 2021 ·
Published Online: 27 July 2021

Bihan Wang,[1] Nana Li,[1,a)] Yongsheng Zhao,[1] Xuqiang Liu,[1] Mingtao Li,[1] Qian Zhang,[1,2] Haini Dong,[1] Yu He,[3] Dongzhou Zhang,[4] Yonggang Wang,[1] Gang Liu,[1] Youwen Long,[5] and Wenge Yang[1,a)]

AFFILIATIONS

[1]Center for High Pressure Science and Technology Advanced Research (HPSTAR), Shanghai 201203, People's Republic of China
[2]College of Material and Chemical Engineering, Zhongyuan University of Technology, Zhengzhou 450007, People's Republic of China
[3]Key Laboratory of High-Temperature and High-Pressure Study of the Earth's Interion, Institute of Geochemistry, Chinese Academy of Sciences, Guiyang 550081, People's Republic of China
[4]Hawaii Institute of Geophysics & Planetology, University of Hawaii Manoa, Honolulu, Hawaii 96822, USA
[5]Beijing National Laboratory for Condensed Matter Physics, Institute of Physics, Chinese Academy of Sciences, Beijing 100190, People's Republic of China

[a)]**Authors to whom correspondence should be addressed:** nana.li@hpstar.ac.cn and yangwg@hpstar.ac.cn

ABSTRACT

The exploration of next-generation materials and the underlying mechanisms for high ionic conductivity have been the mainstay of the study in the solid state ionic field, but with limited success. Here, we performed closely integrated *in situ* high-pressure structural and electronic characterizations on $SrCoO_{2.5}$, a typical material for solid fuel cell application. We discovered that the activation energy for ionic transport decreased by approximately 47% at 13.6 GPa upon compression, demonstrating a large enhancement of conductivity. Such a desired functional behavior is strongly interlinked with the pressure-driven isostructural phase transition at which negative linear compressibility occurs along *c*-lattice, weakening the interaction between Co and O atoms and then enhancing the ionic diffusion. Our results provide fundamental insight of the solid ionic mechanism and materials-by-design for future high-performance oxides.

Oxygen deficiency strontium cobalt oxides ($SrCoO_{3-\delta}$), which transport ions via the oxygen diffusion mechanism, play a significant role in various energy storage and conversion applications.[1–4] Due to the highly tunable compositional and structural characteristics, the $SrCoO_{3-\delta}$ system features rich and diverse physical properties and, thus, the functional performance. For example, a ferromagnetic–antiferromagnetic phase transition was convinced as perovskite phase $SrCoO_3$ converts to brownmillerite phase $SrCoO_{2.5}$, where the latter is a promising active material for oxygen permeating membranes, sensors, and cathodes in solid oxygen fuel cells (SOFCs).[5–12] The ionic transport behavior in the brownmillerite oxide family including $SrCoO_{2.5}$ and $BaInO_{2.5}$ is strongly dependent on the well-ordered oxygen-vacancy channels and rich polyhedral configurations, which is structurally preferred at elevated temperatures.[13–16] As such, an improvement in ionic conductivity at room temperature (RT) becomes a formidable materials science challenge,[17,18] and understanding the root cause from a structural viewpoint is urgently needed.

As an additional thermodynamic dimension, pressure plays a crucial role in continuously tuning the crystal lattice and electronic wave functions; thus, it has been demonstrated as a powerful and clean tool for materials engineering and reliable detection of structure–property relationships.[19] Pressure also controls various functional materials across conventional barriers between insulators and metals and between order and disorder states.[20,21] Considering that the activation energy and ionic conductivity are highly dependent on the crystalline lattice in oxides,[22–24] pressure engineering could be an alternative route to tune and improve the functionality of SOFC-related materials including the $SrCoO_{3-\delta}$ system. Upon compression, Xu *et al.* observed a pressure-induced semiconductor-to-insulator transition in $Li_{0.9}CoO_2$, which originates from the Co–O bond length

shrinkage in the CoO_6 octahedron.[25] In Li_xFePO_4, pressure-suppressed valence fluctuation with an activation volume for polaron hopping of +5.8 Å^3 was found, accounting for a correlated motion of polarons and Li^+ ions.[26] In addition, Li^+ migration barrier energies along [010] and [001] directions were demonstrated to increase under compression, further suggesting a deterioration of ionic conductivity that is discovered in high-pressure research on Ba–Ce–Y ternary oxides.[27–29]

Previous results imply that pressure usually leads to an increase in the activation energy and, thus, inhibits the ionic conductivity, raising a question that is the pressure engineering truly inapplicable for high-ionic-conductive materials. In this work, by employing advanced synchrotron-based characterizations and the diamond-anvil-cell (DAC) technique, we observed an unusual pressure-induced isostructural phase transition with a negative linear compressibility along the *c*-axis in $SrCoO_{2.5}$. A considerably low activation energy for ionic transport was then convinced at phase transition pressure, ∼13.6 GPa, demonstrating a favored ionic conductive behavior. A detailed analysis on structural evolution is also proposed, promising for future materials design in a broad context.

The $SrCoO_{2.5}$ polycrystalline sample was synthesized by a traditional solid state reaction method. Starting material $SrCO_3$ (≥99.0%) and CoO (≥99.0%) powders were mixed with a 1:1 molar ratio of Sr and Co in an agate mortar with a pestle. The mixtures were thoroughly ground and pressed into pellet and sintered in a muffle furnace at 1000 °C for 24 h, which is followed by furnace cooling with shutting off the power.

Synchrotron angle-dispersive x-ray diffraction (XRD) patterns of $SrCoO_{2.5}$ under high pressure were collected with a wavelength λ of 0.4340 Å at the beamline 13BM-C of the Advanced Photon Source (APS), Argonne National Laboratory (ANL). Two 300 μm culet diamond anvils, a rhenium gasket, and the silicone oil were used in a symmetric diamond anvil cell (DAC) for generating high pressure.[30] The XRD patterns were analyzed with the General Structure Analysis System (GSAS) and graphical user interface EXPGUI package to refine the crystal structures at various pressures.[31]

In the electrical transport measurements, the rhenium gasket chamber was covered by prepressed cubic boron nitride (*c*-BN) powder around the rhenium gasket chamber to ensure insulation. For AC impedance measurements, the two-probe method was used. Two Pt foils (around 100 × 100 μm^2) were placed at the top and bottom of the sample. A Zahner impedance analyzer was utilized to probe the AC impedance spectrum in the frequency range of 0.01 Hz–4 MHz.

Simulation of the AC impedance spectrum with various circuits provides an effective way to explore the electronic and ionic conductive behavior in materials. In general, the ideal impedance spectra of dominant ionic conductors can be readily interpreted by use of the standard Debye circuit and show a straight line named Warburg tail at low frequencies, when an ion blocking electrode is applied.[32–34] Mixed ionic and electronic conductors may also show only one or two semicircles without a Warburg tail.[33,35,36] The arcs in impedance spectra of mixed conductors are asymmetric, exhibiting a characteristic Warburg-like shape that has no low frequency tail, as the interfacial capacitance is shunted by the electronic current at low frequencies.

The AC impedance spectrum at selected pressures and temperatures of $SrCoO_{2.5}$ is shown in Fig. 1. The diameter of the semicircle decreases with the increasing temperature indicating an enhancement in charge/ion carrier density and/or mobility. From previous research, the Brownmillerite $SrCoO_{2.5}$ phase exhibits a semiconducting behavior while the $SrCoO_3$ compound is metallic.[9,37] Electronic and ionic conduction are coexistent in $SrCoO_{2.5}$ at ambient pressures.[38] In our *in situ* high pressure study, both contributions from electronic and ionic conduction can be found between room temperature and 333 K at around 1 GPa as shown in Figs. 1(a) and S1 in the supplementary material, judged by the impedance spectra. In the higher temperature zone (above 330 K) at 1.0 GPa, the AC impedance spectrum of $SrCoO_{2.5}$ shows a dominant ionic conductive behavior since it follows a straight up behavior at the low frequency region[39] as shown in Fig. 1(a). As pressure increases, the ionic conductivity is gradually suppressed untill 8.2 GPa, where the Warburg tail at low frequency has already disappeared at room temperature [Fig. 1(c)]. As temperature increases, instead, a mixture of ionic and electronic conduction can be seen at the highest temperature 353 K. This can be understood as the decreasing interatomic distance makes the migration of oxygen ions more difficult, thus reducing the oxygen ion conductivity upon compression. Unexpectedly, at 13.6 GPa after the structural phase transition takes place around 10 GPa, AC impedance spectroscopy shows the re-emergent of a mixture of ionic and electronic conducting behaviors at room temperature. Importantly, the dominant ionic conduction can be observable at 353 K. The structural investigation indicates that this enhancement of the ionic conductivity originates from a structural phase transition occurring at around 10 GPa, which will be discussed later. Upon further compression up to 22.6 GPa, the ionic conduction is suppressed again at higher pressures as shown in Fig. 1(f).

To make more quantitative analyses, the impedance data were modeled by one equivalent series circuit consisting of the resistor (R), the constant phase element (CPE), and the Warburg element (W).[40] Using ZView impedance analysis software,[41] we fitted the data and obtained the grain and grain boundary contribution to the AC resistance at various pressures and temperatures. For the impedance spectrum with the Warburg tail of dominant ionic conductivity in $SrCoO_{2.5}$, we used two RC elements connected in series and one Warburg element in series as an equivalent circuit to fit. For a mixed electronic and ionic conductor, two RC elements connected in series were used to fit the impedance plots. The resistance obtained from two RC elements is from the bulk and grain boundary. The equivalent circuits are shown in Figs. S1(b) and S1(c). We present two typical fitting results for 303 and 343 K measurements at 1.0 GPa in Fig. S1. Total resistivity including bulk and grain boundary parts vs pressure at room temperature (RT) is plotted in Fig. S2. It turns out that there is a sharp drop in resistivity around 10 GPa, where the structural phase transition takes place.

More physical insights into the conductive mechanism were obtained from the analysis of the activation energy E_a, a key parameter in all thermally activated processes, which refers to the energy barrier that a system needs to overcome for the process to take place. For ionic diffusion, the relationship between E_a and ionic conductivity can be described by the Arrhenius equation[42,43]

$$\sigma T = \sigma_0 \exp\left(\frac{-E_a}{k_B T}\right), \tag{1}$$

where σ is the ionic conductivity at given temperature T, k_B is Boltzmann constant, and σ_0 is a temperature independent pre-factor.

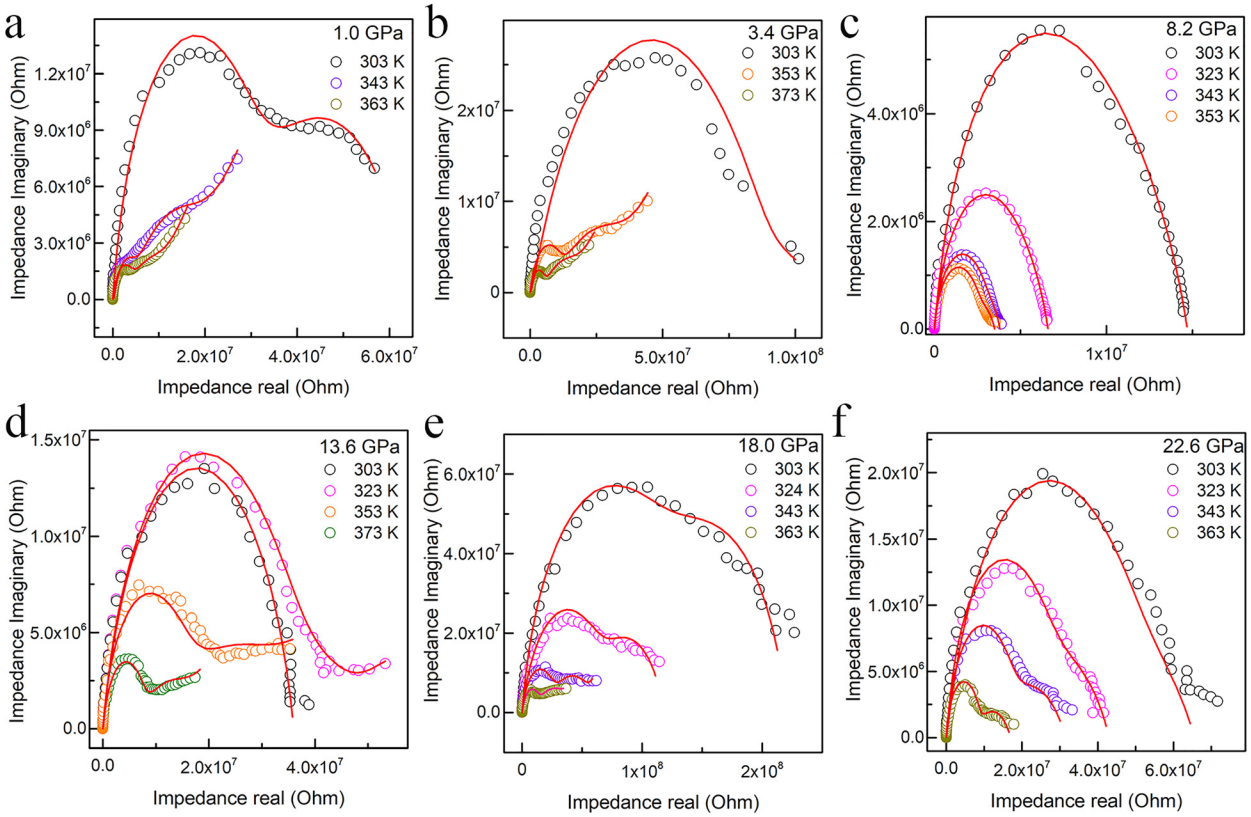

FIG. 1. AC impedance spectrum of $SrCoO_{2.5}$ at selected pressures and temperatures. Panels of (a), (b), (c), (d), (e), and (f) are the AC impedance spectrum at 1.0, 3.4, 8.2, 13.6, 18.0, and 22.6 GPa at temperatures between 303 and 373 K, respectively. The solid lines are the fitting results by the equivalent circuit.

Here, we employed resistivity ρ ($\rho = 1/\sigma$) in Eq. (1) to calculate E_a. Figures 2(a) and 2(b) show ln(ρ/T) vs 1/T at pressures 5.9 and 13.6 GPa, respectively. There are two distinguished segments in $\ln(\rho/T)$ vs $1/T$. Considering the fact that at high temperatures the ionic conductive mechanism dominates the whole transport process, we fit the data points obtained above 324–334 K to estimate the activation energy describing the ionic contribution (denoted as E_{ai}) and that at a low temperature range (up-right data points) related to the mixture contribution from ionic and electric transport mechanisms (denoted as E_a). At 5.9 GPa, the E_{ai} and E_a are 0.53 and 0.28 eV, respectively. At 13.6 GPa, a much lower activation energy contributed from ionic part (E_{ai}) is convinced, being on the order of 0.28 eV. The similar procedure is applied to all measurements up to 22.6 GPa as detailed in Fig. S3 in the supplementary material. The activation energy E_{ai} points are summarized in Fig. 2(c). The activation energy E_{ai} of ionic parts changes from 0.49 eV at 1.0 GPa to 0.53 eV before

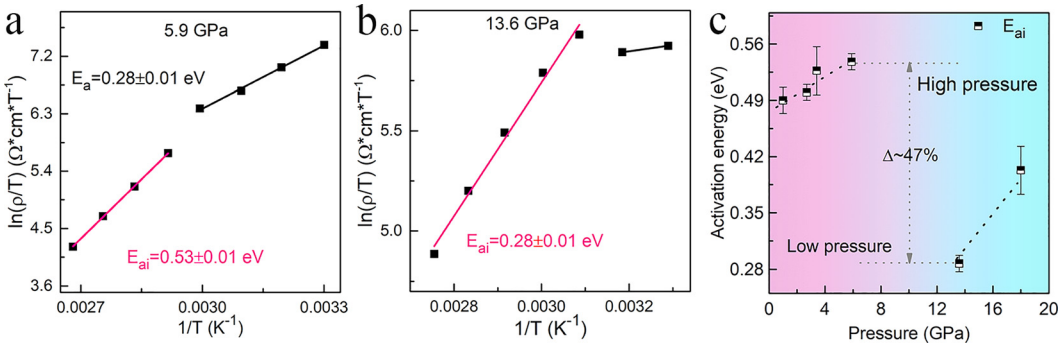

FIG. 2. Arrhenius plot and activation energy E_{ai} in $SrCoO_{2.5}$ at high pressures. (a) and (b) are the fitting results using Eq. (1) from the $\ln(\rho/T)$ vs $1/T$ curves at 5.9 and 13.6 GPa. (c) E_{ai} as a function of pressure.

8.2 GPa, as the interatomic distance decreases with pressure. Surprisingly, the activation energy E_{ai} shows a 47% reduction to 0.28 eV, and overall conductivity improved by an order of magnitude (see Fig. S2 in the supplementary material) at room temperature and 13.6 GPa. At higher pressures above 18 GPa, the ionic conductivity is suppressed again and the E_{ai} increases to 0.40 eV at 18 GPa [see Figs. 1(e) and S3(c)]. Eventually, no dominant ionic conductivity was monitored at all detected temperatures at 22.6 GPa [see Figs. 1(f) and S3(d)].

In the previous study,[44] Gao *et al.* discussed the physical parameters that can affect the ion transport property, including lattice volume, coordination, local disorder and distortion, defects, and lattice dynamics. Among those factors, the effect of lattice volume on ionic conductivity is very obvious in our study, as the activation energy of ionic parts increases with the decreasing of lattice volume before 10 GPa. Previous results suggest a pressure induced phase transition, yet the crucial and detailed structural information of a high pressure phase is not clarified.[45] Nevertheless, the change in coordination and local environment of oxygen ions should largely affect the ion transport channel, which results in a large modification on ionic conductivity. We can analysis those effects from the lattice changes and distortion of the polyhedron. For this, we performed the structural evolution study with applied pressure in $SrCoO_{2.5}$. At ambient pressures, the crystal structure of $SrCoO_{2.5}$ crystalizes in the brownmillerite structure with *Ima*2 space group, which is an ordered oxygen vacancy structure from the perovskite $SrCoO_3$ by removing 1/6 oxygen atoms.[4] Consequently, $SrCoO_{2.5}$ consists of layers of CoO_4 tetrahedra alternating with layers of CoO_6 octahedra along the *a* axis, while the Sr atoms are located in the voids among the polyhedra.[4,10] Here, the *in situ* synchrotron-based XRD measurements on $SrCoO_{2.5}$ were conducted up to 51 GPa, and selected diffraction patterns are displayed in Fig. 3(a). No new diffraction peaks emerged up to the highest pressure we reached. However, the relative intensities and positions of lattice planes (411) and (002) showed a sharp change around 10 GPa. To obtain the accurate atomic positions, we carried out the Rietveld refinements to all the XRD patterns. Two typical profiles at 2.3 and 21.9 GPa are shown in Fig. 3(b). Although the crystalline symmetry remains the same, both lattice parameters and unit cell volume show a discontinuity at 10 GPa [Figs. 3(c) and 3(d)]. The *a*-lattice shortens sharply while the *c*-lattice shows an anomalous expansion. Overall, a substantial volume collapses about 1.8% at 10 GPa, signifying the occurrence of a typical first-order isostructural phase transition. It should be noted that this transition is reversible upon released pressure. We fit experimental *P*–*V* data by a third-order Birch–Murnaghan equation of state (EOS).[46] Below 10 GPa, we obtained volume $V_0 = 474.12$ Å^3, bulk modulus $B_0 = 91(4)$ GPa, and its pressure derivative $B'_0 = 9.5$. For the high-pressure phase, it yields $V_0 = 462.44$ Å^3 and $B_0 = 153(4)$ GPa with $B'_0 = 5.5$.

We then consider the effect of such a first-order isostructural transition and the *c*-lattice expansion on the conduction property. Figure 4(a) depicts the distinctive atomic structures of brownmillerite $SrCoO_{2.5}$ from the cubic $SrCoO_3$. Clearly, after the removal of 1/6 oxygen atoms from $SrCoO_3$, a distinguished open diffusion channel for oxygen ions along the [001] direction can form in brownmillerite phase $SrCoO_{2.5}$. We then consider the pressure dependence of the bonding length and angles between Co and O atoms. According to the refinements of XRD patterns, it is clear that applying pressure has a significant impact on both bond lengths and bond angles of the CoO_4

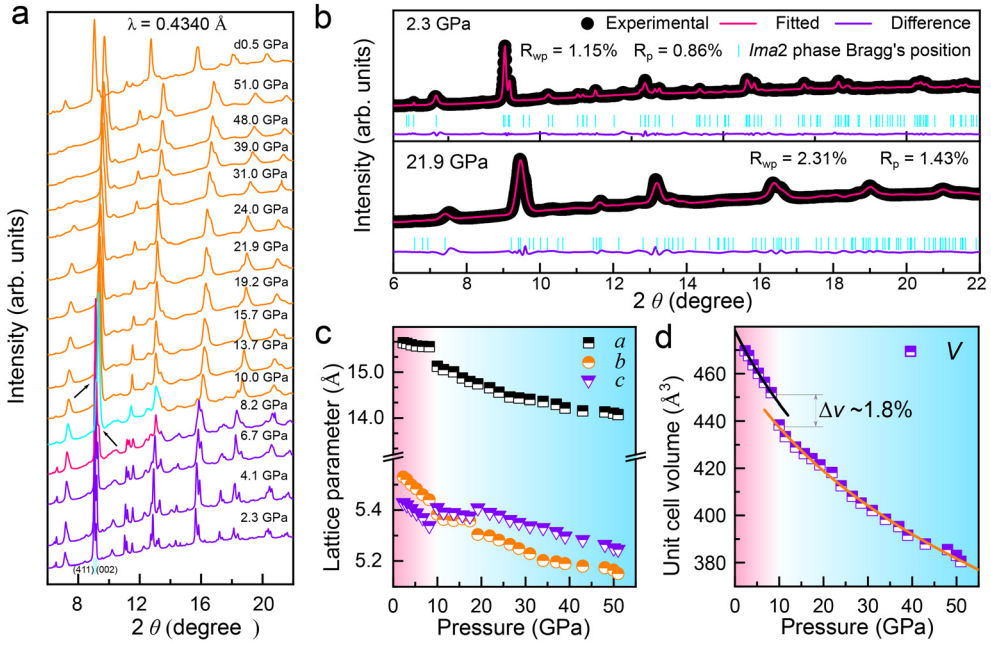

FIG. 3. Structural evolution of $SrCoO_{2.5}$ under high pressure probed by synchrotron x-ray diffraction. (a) Selected x-ray diffraction patterns at room temperature and high pressures. Incident x-ray wavelength is $\lambda = 0.4340$ Å. (b) Representative Rietveld refinement profiles at 2.3 and 21.9 GPa. (c) Lattice parameters vs pressure. (d) *P*–*V* equation of state up to 51 GPa.

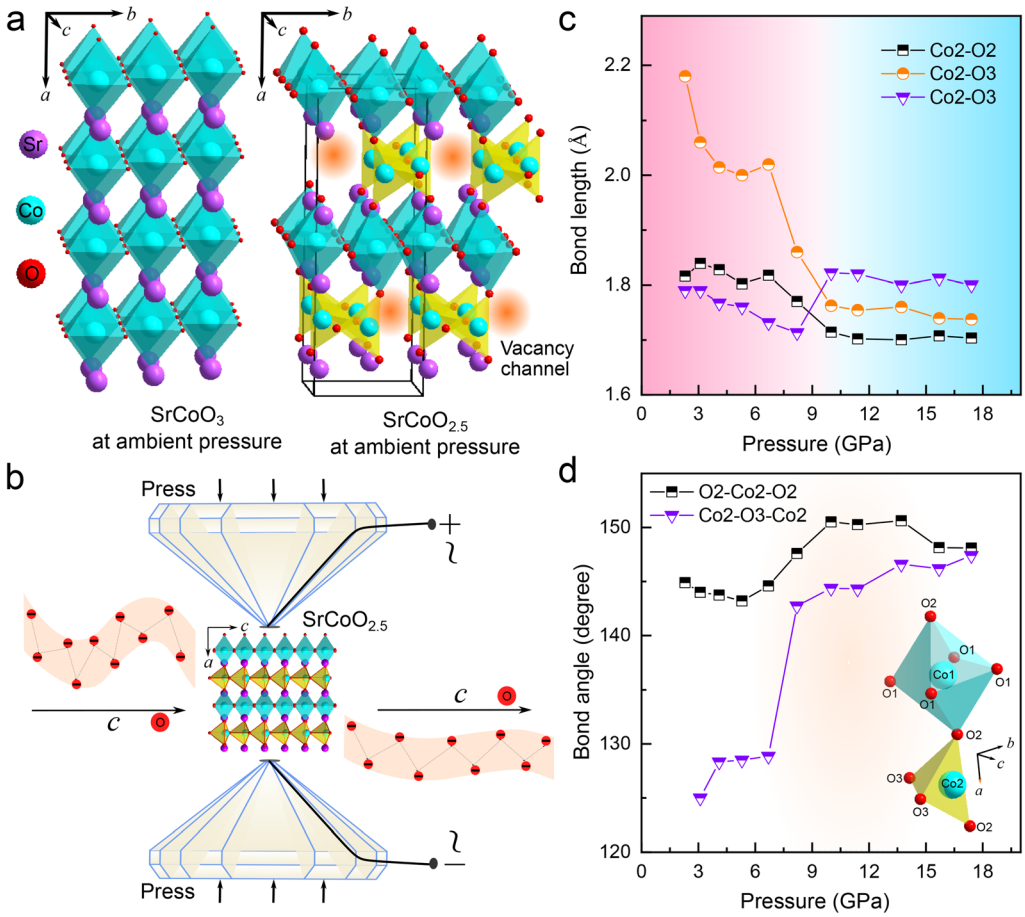

FIG. 4. Bond length and bond angle of CoO_4 tetrahedra in $SrCoO_{2.5}$ at high pressures. (a) Crystal structures of $SrCoO_3$ and $SrCoO_{2.5}$. Red filled circles indicate the ordered vacancy channels for oxygen ion diffusion. (b) Sketch of the pressure effect on the ionic conducting channel. (c) Bond lengths of Co–O in CoO_4 tetrahedra at different pressures. (d) Bond angles of O_2-Co_2-O_2 and Co_2-O_3-Co_2 in CoO_4 tetrahedra at different pressures.

tetrahedra [Figs. 4(c) and 4(d)] vs pressure extracted from the Rietveld refinements. Co_2-O_3 bond length shows a sharp drop at around 10 GPa accompanying by an apparent increase in the bond angle of Co_2-O_3-Co_2 and O_2-Co_2-O_2. These changes in the bond length and the bond angle weaken the distortion of CoO_4 tetrahedra, which potentially increases the overlap of the Co^{3+} *3d* and O^{2-} *2p* orbitals.[1] Also, the stretching along the *c*-axis induces a weaker interaction between Co and O atoms, which would enhance the ionic diffusion along this direction. As a result, it promotes the oxygen diffusion between two CoO_4 tetrahedra along the *c*-axis, leading to the decrease in the activation energy and improvement in ionic conductivity. Figure 4(b) sketches the pressure-effect on the ionic conducting channel before and after the phase transition triggered by applying external pressure.

In conclusion, combining multiple *in situ* high-pressure with high-temperature characterization tools, we investigated the structural and ionic transport properties of $SrCoO_{2.5}$. The pressure-induced first order isostructural phase transition was observed around 10 GPa accompanied by unusual *c*-lattice expansion and suppressed distortion of CoO_4 tetrahedra, decreasing the activation energy by 47% and largely enhancing the ionic conductivity. Our study demonstrates that the high pressure regulating effect on the lattice can largely enhance the ionic conductivity from a phase transition mechanism, contrary to common belief; thus it should be paid attention in the future. We also expect the lattice expansion induced activation energy suppression for better ionic conductive materials and device performance could be extended to other oxide families beyond $SrCoO_{2.5}$.

See the supplementary material for the fit of the experimental AC impedance data at 1.0 GPa and the resistivity of $SrCoO_{2.5}$ at high pressure and room temperature.

AUTHORS' CONTRIBUTIONS

B.W. and N.L. contributed equally to this work.

This work was financially supported by the National Nature Science Foundation of China (Grant Nos. 51527801, 51772184, U1930401, and U2032129). *In situ* high-pressure x-ray diffraction measurements were performed at GeoSoilEnviroCARS (The University of Chicago, Sector 13), Advanced Photon Source (APS), Argonne National Laboratory. GeoSoilEnviroCARS was supported

by the National Science Foundation-Earth Sciences (No. EAR-1634415) and Department of Energy-GeoSciences (No. DE-FG02–94ER14466). This research used the resources of the Advanced Photon Source, a U.S. Department of Energy (DOE) Office of Science User Facility operated for the DOE Office of Science by Argonne National Laboratory under Contract No. DE-AC02–06CH11357.

DATA AVAILABILITY

The data that support the findings of this study are available from the corresponding authors upon reasonable request.

REFERENCES

[1]C. de la Calle, A. Aguadero, J. A. Alonso, and M. T. Fernandez-Diaz, Solid State Sci. **10**, 1924–1935 (2008).
[2]N. Lu, P. Zhang, Q. Zhang, R. Qiao, Q. He, H.-B. Li, Y. Wang, J. Guo, D. Zhang, Z. Duan, Z. Li, M. Wang, S. Yang, M. Yan, E. Arenholz, S. Zhou, W. Yang, L. Gu, C.-W. Nan, J. Wu, Y. Tokura, and P. Yu, Nature **546**, 124–128 (2017).
[3]Q. Lu and B. Yildiz, Nano Lett. **16**, 1186–1193 (2016).
[4]Q. Yang, H. Cho, H. Jeem, and H. Ohta, Adv. Mater. Interfaces **6**, 1901260 (2019).
[5]Y. Long, Y. Kaneko, S. Ishiwata, Y. Taguchi, and Y. J. Tokura, J. Phys.: Condens. Matter **23**, 245601 (2011).
[6]H. Jeen, W. S. Choi, J. W. Freeland, H. Ohta, C. U. Jung, and H. N. Lee, Adv. Mater. **25**, 3651–3656 (2013).
[7]T. Takeda, H. Wantanabe, and Y. Yamaguchi, J. Phys. Soc. Jpn. **33**, 970 (1972).
[8]H. Taguchi, M. Shimada, and M. Koizumi, J. Solid State Chem. **29**, 221 (1979).
[9]P. Bezddicka, A. Wattiaux, J. C. Grenier, M. Pouchard, and P. Hagenmuller, Z. Anorg. Allg. Chem. **619**, 7 (1993).
[10]R. Le Toquin, W. Paulus, A. Cousson, C. Prestipino, and C. Lamberti, J. Am. Chem. Soc. **128**, 13161 (2006).
[11]H. Jeen, W. S. Choi, M. D. Biegalski, C. M. Folkman, I. C. Tung, D. Fong, J. W. Freeland, D. Shin, H. Ohta, M. F. Chisholm, and H. N. Lee, Nat. Mater. **12**, 1057 (2013).
[12]J. Fleig and J. Maier, J. Eur. Ceram. Soc. **24**, 1343 (2004).
[13]K. Gupta, S. Singh, and M. S. R. Rao, J. Nanosci. Lett. **3**, 12 (2013).
[14]A. Muñoz, C. de la Calle, J. A. Alonso, P. M. Botta, V. Pardo, D. Baldomir, and J. Rivas, Phys. Rev. B **78**, 054404 (2008).
[15]J. B. Goodenough, J. E. Ruiz-Diaz, and Y. S. Zhen, Solid State Ion. **44**, 21 (1990).
[16]T. R. S. Prasanna and A. Navrotsky, J. Mater. Res. **8**, 1484 (1993).
[17]T. Famprikis, P. Canepa, J. A. Dawson, and M. S. Islam, Nat. Mater. **18**, 1278–1291 (2019).
[18]A. Aguadero, L. Fawcett, S. Taub, R. Woolley, K. Wu, N. Xu, J. A. Kilner, and S. J. Skinner, J. Mater. Sci. **47**, 3925–3948 (2012).
[19]G. Liu, L. P. Kong, W. G. Yang, and H. K. Mao, Mater. Today **27**, 91–106 (2019).
[20]L. P. Kong, J. Gong, Q. Y. Hu, F. Capitani, A. Celeste, T. Hattori, A. Sano-Furukawa, N. Li, W. G. Yang, G. Liu, and H. K. Mao, Adv. Funct. Mater. **31**, 2009131 (2021).
[21]C. S. Yoo, Matter Radiat. Extremes **5**, 018202 (2020).
[22]K. J. Laidler, J. Chem. Educ. **61**, 494 (1984).
[23]S. B. C. Duval, P. Holtappels, U. F. Vogt, U. Stimming, and T. Graule, Fuel Cells **9**, 613 (2009).
[24]S. Ricote, N. Bonanos, A. Manerbino, and W. G. Coors, Int. J. Hydrogen Energy **37**, 7954–7961 (2012).
[25]C. Xu, W. Xiao, T. Liu, F. Sun, J. Zheng, S. Peng, X. Liu, F. Pan, W. Yang, and H. K. Mao, J. Mater. Chem. A **5**, 19390–19397 (2017).
[26]S. J. Tracy, L. Mauger, H. J. Tan, J. A. Munoz, Y. Xiao, and B. Fultzi, Phys. Rev. B **90**, 094303 (2014).
[27]H. Dong, H. Guo, Y. He, J. Gao, W. Han, X. Lu, S. Yan, K. Yang, H. Li, D. Chen, and H. Li, Solid State Ion. **301**, 133–137 (2017).
[28]Q. Chen, T. Huang, M. Baldini, A. Hushur, V. Pomjakushin, S. Clark, W. L. Mao, M. H. Manghnani, A. Braun, and T. Graule, J. Phys. Chem. C **115**, 24021–24027 (2011).
[29]Q. Chen, A. Braun, S. Yoon, N. Bagdassarov, and T. Graule, J. Eur. Ceram. Soc. **31**, 2657–2661 (2011).
[30]H. K. Mao, "Design and varieties of the megabar cell," Carnegie Inst. Washington Yearb. **77**, 904–908 (1978).
[31]A. C. Larson and R. B. Von Dreele, "General structure analysis system (GSAS)," Los Alamos National Laboratory Report No. LAUR 86-748 (2004).
[32]R. A. Huggins, Ionics **8**, 300–313 (2002).
[33]W. Lai and S. M. Haile, J. Am. Ceram. Soc. **88**, 2979 (2005).
[34]J. T. S. Irvine, D. C. Sinclair, and A. R. West, Adv. Mater. **2**, 132 (1990).
[35]R. Amin and Y. M. Chiang, J. Electrochem. Soc. **163**, A1512 (2016).
[36]J. Zahnow, T. Bernges, A. Wagner, N. Bohn, J. R. Binder, W. G. Zeier, M. T. Elm, and J. Janek, ACS Appl. Energy Mater. **4**, 1335 (2021).
[37]S. Balamurugan, K. Yamaura, A. B. Karki, D. P. Young, M. Arai, and E. Takayama-Muromachi, Phys. Rev. B **74**, 172406 (2006).
[38]A. M. Narayanan and A. M. Umarji, J. Alloys Compd. **803**, 102–110 (2019).
[39]J. Wang, Y. Hao, H. Liu, G. Zhang, C. Liu, and C. Gao, Phys. Chem. Chem. Phys. **20**, 7492–7497 (2018).
[40]D. C. Sinclair and A. R. West, J. Appl. Phys. **66**, 3850 (1989).
[41]D. Johnson, *ZView: A Software Program for IES Analysis, Version 2.8* (Scribner Associates, Inc., Southern Pines, NC, 2008), p. 200.
[42]H. Trabelsi, M. Bejar, E. Dhahri, M. Sajieddine, K. Khirouni, P. Prezas, B. Melo, M. Valente, and M. Graça, J. Alloys Compd. **723**, 894–903 (2017).
[43]A. Pelaiz-Barranco, J. Guerra, R. Lopez-Noda, and E. Araujo, J. Phys. D **41**, 215503 (2008).
[44]Y. Gao, A. M. Nolan, P. Du, Y. Wu, C. Yang, Q. Chen, Y. Mo, and S. Bo, Chem. Rev. **120**, 5954–6008 (2020).
[45]F. Hong, B. Yue, Z. Liu, B. Chen, and H. K. Mao, Phys. Rev. B **95**, 024115 (2017).
[46]H. K. Mao, T. Takahashi, W. A. Bassett, G. L. Kinsland, and L. Merrill, J. Geophys. Res. **79**, 1165–1170, https://doi.org/10.1029/JB079i008p01165 (1974).